Journal of Materials Chemistry A

Accepted Manuscript

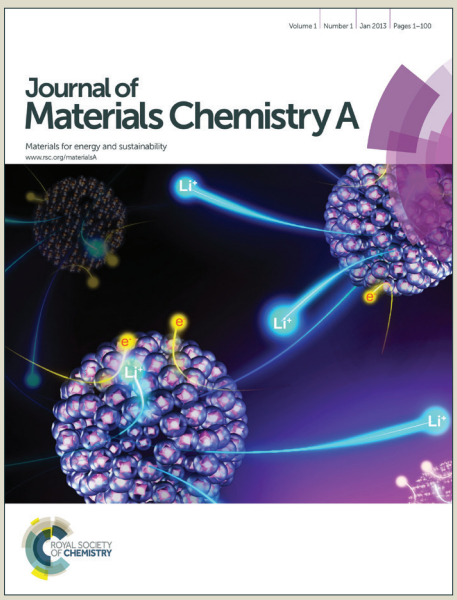

ROYAL SOCIETY OF CHEMISTRY

www.rsc.org/materialsA

Cite this: DOI: 10.1039/c0xx00000x

www.rsc.org/xxxxxx

ARTICLE TYPE

High performance porous $LiMnPO_4$ nanoflake: synthesis from a novel nanosheet precursor

Qingbo Xia,[ab] Tao Liu,[a] Jingjing Xu,[a] Xueyuan Cheng,[ab] Wei Lu[a] and Xiaodong Wu*[a]

Received (in XXX, XXX) Xth XXXXXXXXX 20XX, Accepted Xth XXXXXXXXX 20XX

DOI: 10.1039/b000000x

Micro-sized porous $LiMnPO_4$ nanoflakes constituted by interconnected small-sized $LiMnPO_4$ nanocrystals, were synthesized using the novel precursor of $(C_2N_2H_{10})$ Mn_2 $(PO_4)_2$-$\cdot 2H_2O$ nanosheets through a facile process. After carbon coating, the $LiMnPO_4$-C presents promising electrochemical properties. The strategy described in this work could be helpful for practical application of $LiMnPO_4$.

1. Introduction

The lithium ion batteries (LIBs) with high energy and power density, low cost, and high safety is strongly required for their new applications such as in electric vehicles (EV) and hybrid electric vehicle (HEV).[1-3] The performance of LIBs is largely determined by the capacity and potential of cathode in the battery system, thus developing advanced cathode materials is highly demanded. Olivine-structured phosphates are considered to be the most suitable cathode materials for power batteries owing to their excellent thermal and electrochemical stability.[4-7] To date, olivine $LiFePO_4$ has already been commercialized, but its low operating voltage (3.4 V *vs.* Li) limits its energy density (578 $Wh\cdot kg^{-1}$), which is insufficient for high power applications.[8] Recently, olivine $LiMnPO_4$ has attracted increasing attention as it has a higher voltage (4.1 V *vs.* Li) than, and similar capacity to, $LiFePO_4$. However, the inherently low electronic and ionic conductivities of $LiMnPO_4$ seriously limit electron transport and Li^+ insertion/extraction in this material, making it challenging to achieve high rate capability.[4,8] Effective strategies to overcome these limitations have focused on carbon coating,[2,9,10,11] ion-doping,[12-14,15] Fe-substitution,[5,16,17] and reducing crystallite size to tiny nanoscale.[2,7,18] According to the literature, it is noted that the rate capability of $LiMnPO_4$ could not be significantly increased without a small crystallite size and uniform carbon coating.

The main approaches to obtain tiny $LiMnPO_4$ nanocrystallites, which have been reported, can be divided into two categories: i) using hydrothermal/ solvothermal,[6,11,19] Sol-gel,[20] template,[21] and ultrasonic pyrolysis[22] methods to prepare nano-sized $LiMnPO_4$ particles; and ii) manufacturing the micro/nano-structures of $LiMnPO_4$, and majority of these work focusing on preparing porous $LiMnPO_4$ microspheres using a spherical $MnPO_4\cdot H_2O$ precursor.[5,23] The nano-sized particles remarkably improve the rate capability of $LiMnPO_4$, but the synthetic routes are still expensive and difficult for mass production.[24] Besides, the aggregates of nano-sized particles are always shapeless and incompact that causes their low tap densities and low volumetric energy density.[5] Consequently, the nano-sized LiMnPO4 has been regarded as not suitable for LIBs designed for application in EV and HEV.[5,24] For the porous microspheres, it is believed that that can easily close packed thus have a high tap densities.[25] However, their capacities have been found that was limited by insufficient carbon coating and wetting of electrolyte. The inner part of microsphere is easy to be isolated from the carbon sources and electrolyte due to its isotropous micrometer size scale, resulting in electrochemically inactive area. Therefore, it is a still great challenge to synthesize tiny $LiMnPO_4$ nanocrystallites with high capacity and the favorable particle morphology which is easy to carry out uniform carbon coating and close packing through low cost methods.

In this communication, we report a micro-sized porous $LiMnPO_4$ nanoflake constituted by interconnected $LiMnPO_4$ nanocrystals (30~50 nm), which is transformed from an easy-obtained novel precursor of $(C_2N_2H_{10})Mn_2(PO_4)_2\cdot 2H_2O$ (CMP) nanosheet through sintering that with $LiCH_3COO\cdot 2H_2O$ (LiAc) at 350℃. Obviously, the porous nanoflake is an ideal morphology for inner nanocrystals in favor of carbon coating and wetting since short diffusion distance for carbon source and electrolyte in thickness direction. Besides, the micro-sized flake can also easily form close packed arrays, as with micro-sized sphere, and thus it has a high tap density.

2. Experiment

Preparation of CMP nanosheets: $MnSO_4\cdot H_2O$ and H_3PO_4 were sequentially dissolved in distilled water with a molar ratio of 1:1.2. Next, ethylene-diamine (EN) was added into the mixture solution dropwise until the pH value reaching 9, and the mixture was then stirred for 2 hours. Light pink precipitate of CMP was obtained after filtering and washing with distilled water several times. Finally, the precipitate was dried at 80℃ for a night.

Preparation of porous $LiMnPO_4$-C nanoflakes: The precursor CMP was mixed with stoichiometric LiAc through dispersing them in alcohol by ultrasonic wave. Porous $LiMnPO_4$ nanoflakes were obtained by sintering the mixture at 350℃ for 10 h under N_2 atmosphere. The $LiMnPO_4$-C were obtained by blending $LiMnPO_4$ and glucose in a weight ratio of 10:3 and heating at 650°C for 3 h under nitrogen flow.

Materials characterization: The crystallographic structures of all products were characterized by XRD (D8 Advance, Bruker AXS), and their morphologies were investigated by SEM (S4800, Hitachi). Thermo gravimetric analysis (TG/DTA6200, SII) was used to study the decomposition of CMP. Besides, the $LiMnPO_4$-

C was also characterized by TEM (Tecnai G2 F20 S-Twin, FEI) for its morphology and the thickness of carbon coating layer, and BET (ASAP 2020, Micromeritics) for its special surface area and pore size, and Elementar (Vario EL III) for its carbon content, and a tap density meter (BT301) for its tap density.

Electrochemical Performance Tests: Electrochemical properties of the porous $LiMnPO_4$-C nanoflakes were assessed using CR2025 coin-type cells. The cathode slurry was prepared by mixing the $LiMnPO_4$-C (75 *wt.* %), multiwalled carbon nanotubes (MWCNTs, 5 *wt.* %), acetylene black (AB, 10 *wt.* %) and polyvinylidene fluoride (PVDF, 10 *wt.* %) in n-methyl-2-pyrrolidone (NMP). Al foils were coated with the slurry and dried at 100 ℃ under vacuum for 10h. The cells were formed using Li metal anodes, and the electrolyte of 1M $LiPF_6$ in 1:1:1 mixture solvents of ethylene carbonate (EC), diethyl carbonate (DEC) and dimethyl carbonate (DMC). The cells were cycled on a multi-channel battery cycler (Neware BTS2300). During the test, the cells were charged to 4.5 V with various current rates followed by a constant voltage process until the current dropped to 0.02 C, and then discharged with same rates with charge to 2V.

3. Results and Discussion

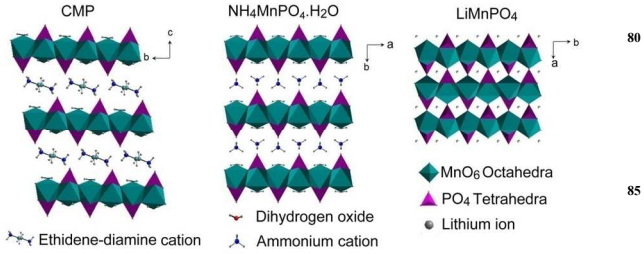

Fig. 1 Crystal structures of $(C_2N_2H_{10})Mn_2(PO_4)_2{\cdot}2H_2O$ (left), $NH_4MnPO_4{\cdot}H_2O$ (middle), and $LiMnPO_4$ (right).

Table 1 The unit cell volume references from the ICSD.

	Space group	Volume of a $XMnP_4$ ($Å^3$)	Reference
$(C_2N_2H_{10})Mn_2(PO_4)_2{\cdot}2H_2O$	P1	135.62	ICSD #102302
$LiMnPO_4$	Pmna	82.81	ICSD #99858

Notes: ICSD stands for the inorganic crystal structure database. $XMnPO4$ is the average unit that contains single $MnPO_4$ in the crystal cell of $(C_2N_2H_{10})Mn_2(PO_4)_2{\cdot}2H_2O$ and $LiMnPO_4$.

$(C_2N_2H_{10})Mn_2(PO_4)_2{\cdot}2H_2O$ (CMP) was first reported by Song and his coworkers in 2003.[26] As shown in Fig. 1, CMP has a typical layered structure, as with $NH_4MnPO_4{\cdot}H_2O$, which can be viewed as manganese (II) phosphate layers being assembled by EN (ammonia in $NH_4MnPO_4{\cdot}H_2O$) through the bonding of N···H···O and O···H···O. CMP crystallizes in triclinic space group P1 rather than ($NH_4MnPO_4{\cdot}H_2O$ crystallizes in) orthorhombic space group Pmn21, probably because EN introduces geometric constraints and lowers the symmetry. $NH_4MnPO_4{\cdot}H_2O$ has been reported in the literatures as a desirable precursor for preparing $LiMnPO_4$ owing to the similarity of their structures.[7,27] The MnO_6/PO_4 layers in $NH_4MnPO_4.H_2O$ structure can be described as the fragments of the structure of $LiMnPO_4$.[28] This similarity allows a transformation from $NH_4MnPO_4{\cdot}H_2O$ into $LiMnPO_4$ without major structural rearrangement and that can achieve under relatively mild conditions.

Therefore, CMP might have been transformed into $LiMnPO_4$ under mild conditions due to its similar structure with $NH_4MnPO_4{\cdot}H_2O$. Besides, as can be seen from Table 1, the unit cell volume of CMP is much larger than $LiMnPO_4$, so there would experience large cell volume shrinkage when CMP transforms into $LiMnPO_4$, and that could make the CMP particle broken.

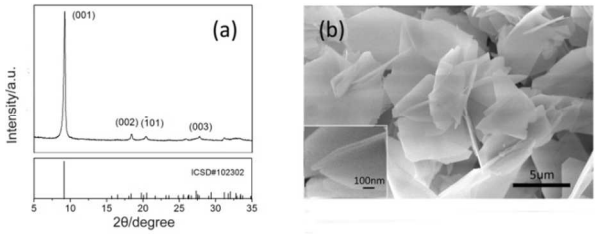

Fig. 2 Characterizations of $(C_2N_2H_{10})Mn_2(PO_4)_2{\cdot}2H_2O$: XRD pattern (a), and SEM images (b).

Owing to week bonding of the N···H···O and O···H···O between MnO_6/PO_4 layers, CMP crystallizes tend to along the MnO_6/PO_4 layer direction, and also similar to $NH_4MnPO_4{\cdot}H_2O$, thus it is easy to obtain the plate-like CMP crystals in a solution reaction system. Fig. 2a shows the XRD pattern of obtained CMP, in which all peaks match well with standard card (the inorganic crystal structure database) ICSD#102302. The diffraction pattern exhibits a dominant (001) peak, indicating the oriented growth of CMP crystals along MnO_6/PO_4 layer direction. Moreover, according to the Bragg equation, the interplanar spacing of (001) facet is 9.6 Å, declaring there are large spaces between MnO_6/PO_4 layers. As can be seen in Fig. 2b, CMP exhibits sheet morphology with a thickness about 60 nm and a lateral size of several micrometers. CMP has a low thermal decomposition temperature, which was illustrated by its TG curve (see Supporting Information Fig. S1). The process of dehydration begins at 100℃, and decomposition of EN begins at 240℃.

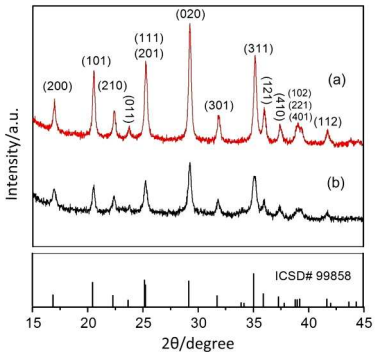

Fig. 3 XRD patterns of $LiMnPO_4$ (a) and $LiMnPO_4$-C (b).

The melting point of LiAc is very low, about 70℃， which is molten before CMP decomposition. So, we supposed whether the free Li^+ from molten LiAc could diffuse into the layer space of MnO_6/PO_4 when H_2O and EN is being released from CMP, as is well known that Li^+ has a very small ionic radius, finally forming the $LiMnPO_4$. The product of CMP nanosheets and LiAc mixture

calcined at 350 ℃ was examined by XRD. XRD pattern (a) in Fig. 3 shows that all diffraction peaks are assigned to orthorhombic $LiMnPO_4$ (space group Pmna(62), ICSD#99858) and no peaks of impurities are detected, which declares that pure olivine $LiMnPO_4$ has been obtained from CMP and LiAc. Moreover, it can be obviously recognized that the highest peak in this pattern is indexed to (020) facet rather than (311) facet in standard card ICSD #99858, and the intensity ratio of I(020)/I(200) = 4.87 is much larger than that of the standard card (I(020)/I(200)= 2.64), which imply the preferred orientation in [010] direction of obtained crystals.[29] It is known that the diffusion pathways of Li^+ are parallel to [010] direction in olivine structure. This orientation means that considerable electrochemical active facets, which parallel to {020} facets, are exposed to the surface of $LiMnPO_4$ crystals. Consequently, abundant active sites of Li^+ insertion/extraction are provided which can accelerate the exchange rate of Li^+ between $LiMnPO_4$ and electrolyte, improving the rate capability of electrode. This character of orientation was still remained after high temperature process of carbon coating that is illustrated by XRD pattern of $LiMnPO_4$-C (pattern (b) in Fig. 3).

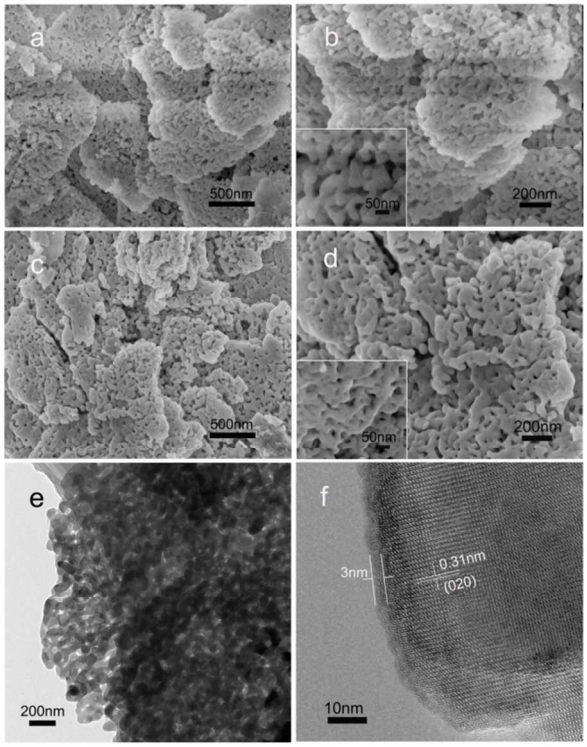

Fig. 4 SEM images of $LiMnPO_4$ (a, b) and $LiMnPO_4$-C (c). TEM image of $LiMnPO_4$-C (e, f).

SEM images in Fig. 4 (a and b) and Fig. S2 (a and b), indicate that the CMP nanosheets have been transformed into porous nanoflakes with a thickness about 80 nm and a lateral size of 1~5 um after reaction with LiAc, which are constituted of interconnected nanoparticles with sizes of 30~50 nm. This change should be caused by large volume shrinkage that has been discussed above, and abundant gas releasing in the transformation process from CMP to $LiMnPO_4$. Massive pores with a width of 20~40 nm in the nanoflakes indicate a good porous structure, which is expected to avail for carbon coating. As can be seen in Fig. 4c and 4d, the porous structure is seldom destroyed by coating carbon. The TEM morphology of single LiMnPO4-C nanoflakes (Fig. 4e) further demonstrates the fine porous structure, which is good for $LiMnPO_4$ wetting by electrolyte sufficiently. The carbon content of LiMnPO4-C is 8.64 *wt.* %, and the TEM image in Fig. 4f indicates a uniform carbon layer of around 3 nm thickness covered on $LiMnPO_4$ nanocrystals. The nitrogen adsorption–desorption measurements (see Fig. S3) were carried out to give a comprehensive description for $LiMnPO_4$ and $LiMnPO_4$-C porous structure sample. The measured BET surface areas of them are 26.2 $m^2 \cdot g^{-1}$ and 17.6 $m^2 \cdot g^{-1}$, respectively. Numerous micropores disappeared after carbon coating, which causes surface area reduced that can be indicated from the difference of pore size distribution (Fig. S3, b and d) between two samples. The average pore diameters of them are all close to 30nm. The tap density of porous $LiMnPO_4$-C nanoflakes is 1.2 $g \cdot cc^{-1}$, which is close to the values measured from high tap density micro-sized porous spheres have been reported, but considerably larger than nanostructured particles (0.3~0.6 $g \cdot cc^{-1}$).[5]

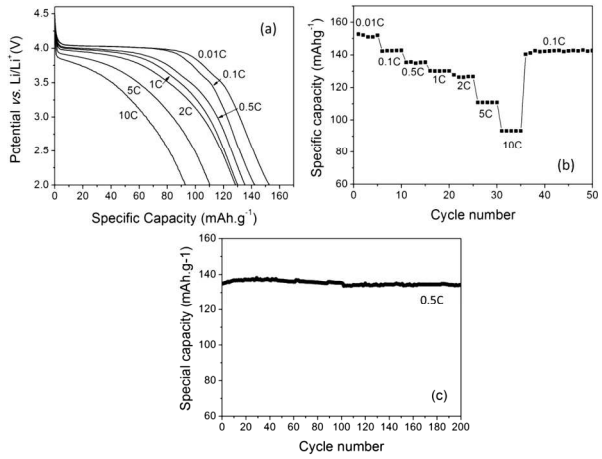

Fig. 5 The electrochemical performance of $LiMnPO_4$-C: (a) the discharge profiles at various rates, (b) the rate capability and (c) the cycling performance.

The electrochemical performance of porous $LiMnPO_4$-C nanoflakes is shown in Fig. 5. All specific capacity values were evaluated including the mass of the coating carbon. The discharge curves at various current densities from 0.01 C to 10 C are shown in Fig. 5a. The flat discharge voltage plateaus decline and shorten with increasing of the rates. However, it is noted that the voltage drop trend is a curve at 10C rather than a skew line with a large slope that occurred in many literatures,[6, 10] showing a good rate capability of this material. Moreover, porous $LiMnPO_4$-C nanoflakes exhibited high discharge capacities, as indicated in Fig. 5b. It presented 151 $mAh \cdot g^{-1}$, 142 $mAh \cdot g^{-1}$, 135 $mAh \cdot g^{-1}$, 130 $mAh \cdot g^{-1}$ and 128 $mAh \cdot g^{-1}$ at 0.01 C, 0.1 C, 0.5 C, 1 C and 2 C, respectively. Attractively, a high discharge capacity 110 $mAh \cdot g^{-1}$ was still maintained at 5 C, and 92 $mAh \cdot g^{-1}$ at 10 C. When the rate went back to 0.1 C after cycling at 10 C, the capacity immediately recovered to previous level. In addition, the porous

$LiMnPO_4$-C nanoflakes showed a good cycling stability. As shown in Fig. 5c, its capacities show no noticeable fade after cycling over 200 cycles at 0.5 C. The good electrochemical properties of $LiMnPO_4$-C can be attributed to its unique structure. The nanocrystals with small size embedded in nanoflakes shorten the diffusion distance for both Li^+ and electrons. And the preferred (020) orientation makes $LiMnPO_4$ crystals have considerable exposed electrochemical active surface facets that can accelerate Li^+ insertion/ extraction. Besides, the porous nanoflake structure makes $LiMnPO_4$ nanoparticles easy for uniform carbon coating that can significantly enhance the electronic conductivity of $LiMnPO_4$, and it also enhances the wetting for $LiMnPO_4$-C by electrolyte. Furthermore, the large specific surface area provides sufficient contact areas of $LiMnPO_4$/electrolyte that accelerate the Li-migration in the interfaces.

4. Conclusions

In summary, $LiMnPO_4$ with the morphology of porous nanoflakes were successfully prepared using novel precursor CMP nanosheets through a facile process. Meanwhile, the $LiMnPO_4$ nanocrystals embedded in these nanoflakes have very small sizes. This morphology is not only beneficial for carbon coating and electrolyte wetting of $LiMnPO_4$ nanocrystals, but also can guarantee a high tap density. The strategy described in this work could be helpful the development of $LiMnPO_4$ cathode in LIBs.

[a]*i-Lab,Suzhou Institute of Nano-Technology and Nano-Bionics, Chinese Academy of Sciences, Suzhou, 215123, People's Republic of China.*
[b]*Nano Science and Technology Institute, University of Science and Technology of China, Suzhou, 215123, People's Republic of China.*
Email: xdwu2011@sinano.ac.cn.
Electronic Supplementary Information (ESI) available. See DOI: 10.1039/b000000x/

Acknowledgments

We are grateful for the financial support of National Natural Science Foundation of China (No. 51404238), Natural Science Foundation of Jiangsu Province, China (No. BK20130360 and No. BK20130353), and Suzhou Science & Technology Bureau of China (No. ZXG201419).

Notes and references

1 B. Zhao, X. Yu, R. Cai, R. Ran, H. Wang, and Z. Shao, *J. Mater. Chem.*, 2012, **22**, 2900-2907.
2 M. Zhao, Y. Fu, N. Xu, G. R. Li, M. T. Wu and X. P. Gao, *J. Mater. Chem. A*, 2014, **2**, 15070-15077.
3 G. Wu, R. Ran, B. Zhao, Y. Sha, C. Su, Y. Zhou and Z. Shao, *J. Energy Chem.*, 2014, **23**, 363-375.
4 A. Yamada, M. Hosoya, S. C. Chung, Y. Kudo, K. Hinokuma, K. Y. Liu and Y. Nishi, *J. Power Sources*, 2003, **119**, 232-238.
5 Y. K. Sun, S. M. Oh, H. K. Park and B. Scrosati, *Adv. Mater.*, 2011, **23**, 5050-5054.
6 M. K. Devaraju and I. Honma, *Adv. Energy Mater.*, 2012, **2**, 284-297.
7 X. H. Rui, X. X. Zhao, Z. Y. Lu, H. T. Tan, D. H. Sim, H. H. Hng, R. Yazami, T. M. Lim and Q. Y. Yan, *Acs Nano*, 2013, **7**, 5637-5646.
8 V. Aravindan, J. Gnanaraj, Y.-S. Lee and S. Madhavi, *J. Mater. Chem. A*, 2013, **1**, 3518.
9 Z. Bakenov and I. Taniguchi, *J. Power Sources*, 2010, **195**, 7445-7451.
10 Daiwon Choi, Donghai Wang, In-Tae Bae, Jie Xiao, Zimin Nie, Wei Wang, Vilayanur V. Viswanathan, Yun Jung Lee, Ji-Guang Zhang, Gordon L. Graff, Zhenguo Yang, and Jun Liu, *Nano Lett.*, 2010, **10**, 2799-2805.
11 J. L. Liu, X. Y. Liu, T. Huang and A. S. Yu, *J. Power Sources*, 2013, **229**, 203-209.
12 J. F. Ni and L. J. Gao, *J. Power Sources*, 2011, **196**, 6498-6501.
13 G. Yang, H. A. Ni, H. D. Liu, P. Gao, H. M. Ji, S. Roy, J. Pinto and X. Jiang, *J. Power Sources*, 2011, **196**, 4747-4755.
14 C. L. Hu, H. H. Yi, F. X. Wang, S. Y. Xiao, Y. P. Wu, D. Wang and D. L. He, *J. Power Sources*, 2014, **255**, 355-359.
15 Q. Lu, G. S. Hutchings, Y. Zhou, H. L. L. Xin, H. M. Zheng and F. Jiao, *J. Mater. Chem. A*, 2014, **2**, 6368-6373.
16 H. L. Wang, Y. Yang, Y. Y. Liang, L. F. Cui, H. S. Casalongue, Y. G. Li, G. S. Hong, Y. Cui and H. J. Dai, *Angew. Chem. Int. Edit.*, 2011, **50**, 7364-7368.
17 P. J. Zuo, G. Y. Cheng, L. G. Wang, Y. L. Ma, C. Y. Du, X. Q. Cheng, Z. B. Wang and G. P. Yin, *J. Power Sources*, 2013, **243**, 872-879.
18 D. Rangappa, K. Sone, Y. Zhou, T. Kudo and I. Honma, *J. Mater. Chem.*, 2011, **21**, 15813-15818.
19 L. J. Hu, B. Qiu, Y. G. Xia, Z. H. Qin, L. F. Qin, X. F. Zhou and Z. P. Liu, *J. Power Sources*, 2014, **248**, 246-252.
20 S. Zhang, F. L. Meng, Q. Wu, F. L. Liu, H. Gao, M. Zhang and C. Deng, *Int. J. Electrochem. Sc.*, 2013, **8**, 6603-6609.
21 H. Yoo, M. Jo, B. S. Jin, H. S. Kim and J. Cho, Adv. Energy Mater., 2011, 1, 347-351.
22 S. M. Oh, H. G. Jung, C. S. Yoon, S. T. Myung, Z. H. Chen, K. Amine and Y. K. Sun, *J. Power Sources*, 2011, **196**, 6924-6928.
23 T. Liu, J. Xu, B. Wu, Q. Xia and X. Wu, *Rsc Adv.*, 2013, **3**, 13337-13341.
24 W. Liu, P. Gao, Y. Y. Mi, J. T. Chen, H. H. Zhou and X. X. Zhang, *J. Mater. Chem. A*, 2013, **1**, 2411-2417.
25 Chunwen Sun, Shreyas Rajasekhara, John B. Goodenough, and Feng Zhou, *J. Am. Chem. Soc.*, 2011, **133**, 2132-2135.
26 Yanning Song, Peter Y. Zavalij, Natasha A. Chernova, and M. Stanley Whittingham, *Chem. Mater.*, 2003, **15**, 4968-4973.
27 C. Y. Wu, J. Xie, G. S. Cao, X. B. Zhao and S. C. Zhang, *Crystengcomm*, 2014, **16**, 2239-2245.
28 N. N. Bramnik and H. Ehrenberg, *J. Alloy Compd.*, 2008, **464**, 259-264.
29 L. Wang, X. He, W. Sun, J. Wang, Y. Li and S. Fan, *Nano Lett.*, 2012, **12**, 5632-5636.

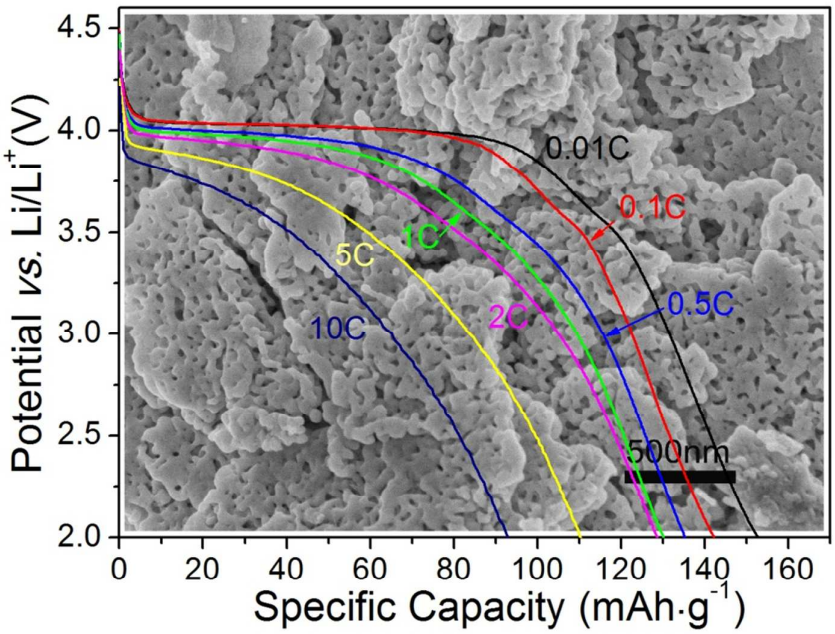

Highlight

1. Micro-sized porous $LiMnPO_4$ nanoflakes were synthesized using a novel precursor.
2. Porous $LiMnPO_4$-C nanoflakes present promising electrochemical properties, especially superior rate capability.
3. The methodology described in this work is facile and would be helpful for practical applications of $LiMnPO_4$ cathode.